

Determinants of Optical Coherence Tomography–Derived Minimum Neuroretinal Rim Width in a Normal Chinese Population

Tin A. Tun,¹ Chen-Hsin Sun,^{2,3} Mani Baskaran,^{1,2,4} Michael J. A. Girard,^{1,5} John Mark S. de Leon,⁶ Ching-Yu Cheng,^{1,2,4} Hla M. Htoon,^{1,2} Tien Y. Wong,^{1,2,4} Tin Aung,^{1,2,4} and Nicholas G. Strouthidis^{1,7,8}

¹Singapore Eye Research Institute and Singapore National Eye Centre, Singapore

²Duke-National University of Singapore (NUS) Graduate Medical School, National University of Singapore, Singapore

³Department of Ophthalmology, National University Health System, Singapore

⁴Department of Ophthalmology, Yong Loo Lin School of Medicine, National University of Singapore, Singapore

⁵In Vivo Biomechanics Laboratory, Department of Biomedical Engineering, National University of Singapore, Singapore

⁶Cardinal Santos Medical Center, Metro Manila, Philippines

⁷National Institute for Health Research (NIHR) Biomedical Research Centre, Moorfields Eye Hospital National Health Service (NHS) Foundation Trust and University College London (UCL) Institute of Ophthalmology, London, United Kingdom

⁸Discipline of Clinical Ophthalmology and Eye Health, University of Sydney, Sydney, New South Wales, Australia

Correspondence: Nick G. Strouthidis, NIHR Biomedical Research Centre at Moorfields Eye Hospital NHS Foundation Trust and UCL Institute of Ophthalmology, 162 City Road, London, EC1V 2PD, UK; nick.strouthidis@moorfields.nhs.uk.

TAT and C-HS are joint first authors.

Submitted: March 3, 2015

Accepted: April 21, 2015

Citation: Tun TA, Sun C-H, Baskaran M, et al. Determinants of optical coherence tomography–derived minimum neuroretinal rim width in a normal Chinese population. *Invest Ophthalmol Vis Sci.* 2015;56:3337–3344. DOI:10.1167/iov.15-16786

PURPOSE. To characterize an optical coherence tomography (OCT)–derived parameter, Bruch’s membrane opening–minimum rim width (BMO–MRW), and its association with demographic and clinical parameters in normal Chinese subjects.

METHODS. Right eyes of 466 consecutive healthy subjects from a population-based study of Singaporean Chinese underwent Cirrus OCT imaging. The retinal internal limiting membrane (ILM) and BMO were automatically delineated using the built-in Cirrus algorithm. The standard 36 interpolated radial B-scans (72 BMO points, 5° increments) of each optic nerve head were manually extracted from the central circle (3.46-mm diameter). We used Matlab to measure the shortest distance from the BMO points to the ILM. Associations of BMO–MRW with demographic and clinical parameters were evaluated using marginal general estimating equations analysis.

RESULTS. There was a slight preponderance of male subjects (50.9%), with a mean age of 54.8 ± 7.63 years. Mean BMO–MRW was 304.67 ± 58.96 μm (range, 173.32–529.23 μm), which was highly associated with OCT-derived disc area (DA) ($\beta = -91.78$, $P < 0.001$) and rim area (RA) ($\beta = 194.31$, $P < 0.001$), followed by spherical refractive error (SRE) ($\beta = -2.23$, $P = 0.02$) and retinal nerve fiber layer (RNFL) thickness ($\beta = 0.5$, $P = 0.04$), after adjusting for the associated factors such as age, sex, intraocular pressure (IOP), and vertical cup–disc ratio (VCDR).

CONCLUSIONS. Disc area and RA had the strongest association with BMO–MRW, followed by SRE and RNFL thickness. The availability of this normative database will facilitate optic nerve head assessment using the BMO–MRW parameter in Chinese subjects.

Keywords: optic nerve head, minimum rim width, vertical cup–disc ratio, optical coherence tomography

The inner edge of Elschnig’s ring (histologically assumed to be the border tissue) is usually defined as the clinical basis for the identification of the optic disc margin. Through imaging the optic nerve head (ONH) using optical coherence tomography (OCT), it is possible to capture surface and nonclinically visible subsurface anatomy objectively.¹ Recent studies have demonstrated that the disc margin, the fundamental landmark in the examination and quantification of optic disc neural rim tissue, does not have a consistent anatomical basis.^{2,3} What the clinician perceives to be the disc margin is therefore not directly comparable to an OCT-derived disc margin, which is based on the innermost edge of Bruch’s membrane (Bruch’s membrane opening, BMO) or retinal pigment epithelium.^{2,3}

The OCT-derived BMO, unlike the clinician-ascribed disc margin, is a consistent landmark that is easily identified and segmented within most OCT volumes. On this basis, the BMO is a suitable landmark from which to define OCT optic disc parameters.

Recently, a previously described parameter^{4–6} defining a neuroretinal rim (NRR) parameter called Bruch’s membrane opening–minimum rim width (BMO–MRW) has been adopted by Reis et al.⁷ This clinically invisible parameter measured by spectral-domain (SD) OCT measures the shortest distance from BMO to the retinal internal limiting membrane (or to the axis of neural tissues) and corresponds closely to the variable trajectory of axons relative to the measurement point, akin to

the method of measuring peripapillary retinal nerve fiber layer (RNFL).⁶ Chauhan et al.⁸ subsequently reported that the BMO-MRW had better diagnostic performance for open-angle glaucoma compared with current disc margin measurements using existing imaging techniques, such as confocal scanning laser tomography and SD-OCT.

Minimum rim area computed from the BMO-MRW is better correlated with RNFL thickness or visual field mean deviation as compared to horizontal rim area at the BMO plane^{9,10} or rim area related to the clinical disc margin.¹¹ However, population-based BMO-MRW normative databases have not been reported yet with large sample sizes. The aim of this study was to investigate normal values of Cirrus OCT-derived BMO-MRW and its association with demographic and clinical parameters in a population-based study of Chinese subjects.

METHODS

Subjects were derived from the Singapore Chinese Eye Study (SCES), a population-based cross-sectional study of ethnic Chinese subjects, aged 40 to 80 years, residing in southwestern Singapore. The recruitment protocol and study design of the SCES have been described in detail elsewhere.¹² In brief, the SCES was conducted to detect the prevalence and impact of major eye diseases among Chinese in Singapore. From 6350 names, an eligibility rate of 70% and a response rate of 75% were assumed to obtain the estimated target sample size of 3300 subjects by using an age-stratified random sampling method. The 3353 participants in SCES represented a 72.8% response rate, and the right eyes of 500 consecutive participants were analyzed in this substudy. Written informed consent was obtained from all participants. The study had the approval of the institutional review board of the Singapore Eye Research Institute and adhered to the tenets of the Declaration of Helsinki.

All participants underwent the following examinations: (1) measurement of visual acuity; (2) refraction using an autokeratometer (RK-5; Canon, Tokyo, Japan); (3) slit-lamp biomicroscopy (model BQ-900; Haag-Streit, Köniz, Switzerland); (4) Goldmann applanation tonometry (AT900D; Haag-Streit); (5) darkroom four-mirror gonioscopy (Ocular Instruments, Inc., Bellevue, WA, USA); (6) standard automated perimetry (SAP) (SITA-Standard 24-2 program; Humphrey Field Analyzer II-750i; Carl Zeiss Meditec, Dublin, CA, USA); and (7) spectral-domain OCT (Cirrus 4000; Carl Zeiss Meditec) imaging after pupillary dilation with tropicamide 1% (Alcon, Puurs, Belgium) on the same day.^{13,14}

The optic disc was evaluated by a trained ophthalmologist using slit-lamp biomicroscopy with measuring graticule (Haag-Streit) during dilated funduscopy using a 78-diopter lens, at $\times 16$ magnification. Vertical disc diameter was measured excluding peripapillary atrophy and the ring of Elschnig. The margins of the optic cup were defined stereoscopically as the point of maximal inflection of vessels crossing the NRR. The vertical cup diameter was measured as the vertical distance between the points of maximum centrifugal extension of the cup between 11 and 1 o'clock and 5 and 7 o'clock. The vertical cup-disc ratio (VCDR) was then calculated. For small optic discs with no visible cup, the measurement was taken as the diameter of the emerging retinal vessels. Disc hemorrhage, notching of the NRR, and thinning of RNFL were documented.

Exclusion Case Definition

Subjects defined as glaucoma or glaucoma suspects were excluded from the study. Glaucoma suspects were defined as those participants fulfilling any of the following criteria: (1)

intraocular pressure (IOP) > 21 mm Hg; (2) VCDR > 0.6 or VCDR asymmetry > 0.2 ; (3) abnormal anterior segment deposit consistent with pseudoexfoliation or pigment dispersion syndrome; (4) narrow anterior chamber angle (posterior trabecular meshwork not seen in ≥ 2 quadrants by darkroom gonioscopy); and (5) peripheral anterior synechiae.

Glaucoma cases were defined by the presence of glaucomatous optic neuropathy (GON), defined as VCDR of > 0.7 and/or NRR narrowing with an associated visual field defect on SAP. The latter was defined if the following were found: (1) glaucoma hemifield test outside normal limits; (2) a cluster of three or more nonedge, contiguous points on the pattern deviation plot, not crossing the horizontal meridian, with a probability of $< 5\%$ being present in age-matched normals (one of which was $< 1\%$); and (3) pattern standard deviation (PSD) < 0.05 ; these were repeatable on two separate occasions, in association with a closed angle (primary angle closure glaucoma, PACG) or with an open angle (primary open-angle glaucoma, POAG). Reliability criteria for SAP were defined as $< 20\%$ fixation losses, $< 33\%$ false-negative error, and $< 33\%$ false-positive error, as recommended by Humphrey Instruments, Inc. (Dublin, CA, USA). We also excluded cases with diabetic retinopathy or optic neuropathies that may account for visual field deficits.

OCT Imaging and Image Processing

Each eye was imaged using the Cirrus OCT optic disc cube 200×200 scan protocol (dimensions, 6×6 mm). Within each volume, the internal limiting membrane (ILM) and retinal pigment epithelium (RPE)/Bruch's membrane complex (BM) were automatically segmented by the Cirrus built-in algorithm. All scans had signal strength ≥ 6 , and there was no motion artifact within the measurement circle (subjective assessment by the authors). The innermost termination of the RPE/BMO was defined as the disc margin, and a plane located 200 μ m above the Bruch's membrane level was defined as the reference plane or the plane separating the NRR from the cup.¹⁵ Cirrus OCT parameters such as mean RNFL thickness, rim area (RA), disc area (DA), and cup volume were computed by the built-in algorithm automatically.

Thirty-six interpolated radial B-scans of each ONH were manually extracted from the central circle (3.46-mm diameter). We developed a customized algorithm, coded in Matlab (Mathworks, Inc., Natick, MA, USA), to measure BMO-MRW automatically. Bruch's membrane opening-MRW is defined as the shortest distance from the BMO point to the ILM (Fig. 1). A constraint was made to ensure that BMO-MRW measurement was within a cylinder, bounded by BMO or within NRR (shaded region, Fig. 1C). The algorithm automatically generated the BMO-MRW values for all 36 B-scans (72 BMO points, 5° increments, commencing at 0°) of an eye, as well as those values for the 4 cardinal B-scans (8 BMO points, 45° increments, commencing at 0°). Six sectoral (temporal, nasal, superior-temporal, superior-nasal, inferior-temporal, and inferior-nasal) and mean BMO-MRW values were correlated with demographic and clinical parameters.

Statistical Analysis

Statistical analyses were performed using IBM SPSS Statistics for Windows (released 2010, Version 19.0; IBM Corp., Armonk, NY, USA). Continuous variables were described as the mean, standard deviation, and range. We used the independent *t*-test to compare the differences in the distribution of continuous variables between two samples and used the χ^2 test for categorical variables. Marginal generalized estimating equations model was used to estimate the relationship between the

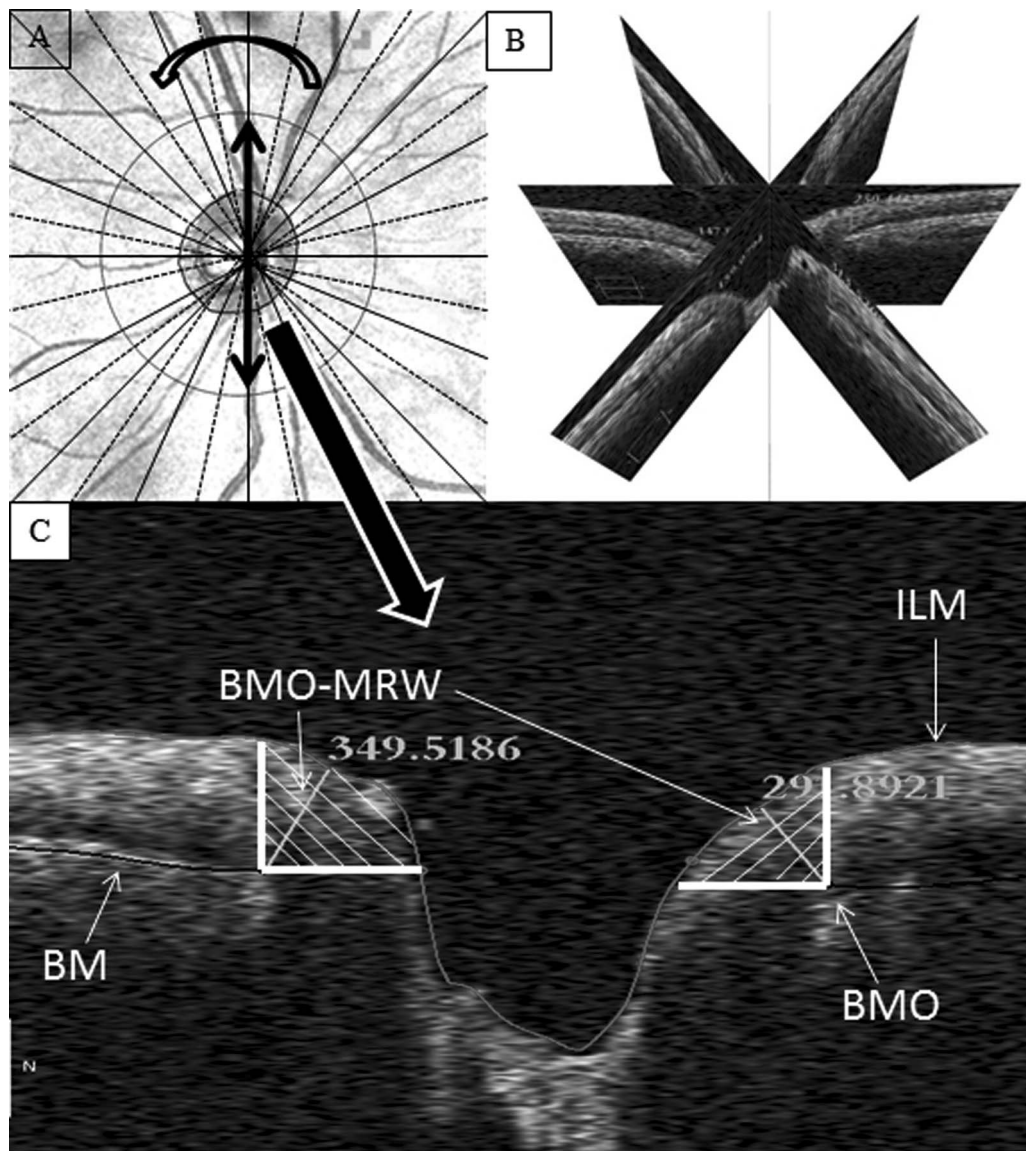


FIGURE 1. Illustration of the method for measuring Bruch's membrane opening-minimum rim width. (A) En face optical coherence tomography fundus image with automatic segmentation of cup-disc. (B) Three-dimensional reconstruction image of optic nerve head. (C) A cross-sectional image of optic nerve head with Bruch's membrane opening-minimum rim width within neuroretinal rim (a cylinder bounded by Bruch's membrane opening, shaded region). BM, Bruch's membrane; BMO-MRW, Bruch's membrane opening-minimum rim width; ILM, internal limiting membrane.

variables. The variables that were significant in univariate analysis were included in multivariate analysis. Analysis of covariance (ANCOVA) with Bonferroni correction was used to obtain the estimated marginal means of BMO-MRW among the sectors after adjusting for age and sex. Comparison of BMO-MRW measurements computed from 36 B-scans and from 4 B-scans was determined by Bland-Altman analysis using MedCalc (Windows v14.12.0; Mariakerke, Belgium). Statistical significance was set at $P < 0.05$.

RESULTS

Of the 500 consecutive recruited subjects, 446 normal subjects were included in the final analysis after 47 glaucoma suspects and 7 glaucoma cases (2 with POAG and 5 with PACG) were excluded. There was a slight preponderance of male subjects (50.9%), and the mean age was 54.8 ± 7.63 years. The

demographic and ONH imaging parameters are summarized in Table 1. Out of the 446 subjects, 368 subjects had performed SAP, and 53 were excluded from analysis due to unreliable SAP results. A total of 315 subjects were therefore included in the univariate analysis to estimate the relationship between BMO-MRW and SAP.

In this cohort, the mean BMO-MRW was 304.67 ± 58.96 μm with range 173.32 to 529.23 μm . Table 2 shows the univariate analysis of factors associated with BMO-MRW, and Table 3 shows multivariate analysis of BMO-MRW after adjustment of associated factors. In univariate analysis, BMO-MRW was highly associated with age ($\beta = -1.29$, $P < 0.001$), VCDR ($\beta = -256.79$, $P < 0.001$), RNFL ($\beta = 1.77$, $P < 0.001$), RA ($\beta = 151.55$, $P < 0.001$), and DA ($\beta = -46.27$, $P < 0.001$), followed by visual field PSD ($\beta = -4.35$, $P = 0.001$), spherical refractive error ($\beta = -4.13$, $P = 0.003$), and sex ($\beta = -13.56$, $P = 0.015$). There was no association of BMO-MRW with systemic factors such as height, weight, and body mass index (BMI)

TABLE 1. Demographic and Imaging Characteristics of All Participants

Variables	Mean, <i>n</i> = 446	Standard Deviation	Range
Age, y	54.8	7.63	44.47 to 81.86
Sex, male:female		227:219	
Pulse pressure, mm Hg	53.49	12.71	21 to 102
Height, cm	164.03	8.43	144 to 190
Weight, kg	63.72	12.59	33.9 to 120.6
BMI, kg/m ²	23.58	3.72	14.49 to 36.77
Spherical refractive error, diopters	-0.39	2.41	-11.75 to 4.75
Intraocular pressure, mm Hg	14	2.7	6 to 22
Axial length, mm	24.02	1.29	21.1 to 28.81
Vertical cup to disc ratio	0.48	0.15	0.05 to 0.83
Mean deviation of standard automated perimetry, dB	-1.71	3.06	-29.75 to 4.09
Pattern standard deviation of standard automated perimetry, dB	2.53	1.94	0.97 to 14.33
Retinal nerve fiber layer thickness, μ m	97.15	10.47	60.53 to 131.86
Disc area, mm ²	1.93	0.37	0.78 to 3.71
Rim area, mm ²	1.29	0.24	0.58 to 2.32
Bruch's membrane opening to minimum rim width, μ m, from 4 B-scans	306.28	61.22	165.13 to 512.5
Bruch's membrane opening to minimum rim width, μ m, from 36 B-scans	304.67	58.96	173.32 to 529.23

TABLE 2. Univariate Analysis of Bruch's Membrane Opening-Minimum Rim Width of Optic Nerve Head

Variables, <i>n</i> = 446	Univariate Analysis of *BMO-MRW ₄		Univariate Analysis of *BMO-MRW ₃₆	
	β (95% CI)	<i>P</i> Value	β (95% CI)	<i>P</i> Value
Age, y	-1.37 (-2.06, -0.68)	<0.001	-1.29 (-1.96, -0.63)	<0.001
Sex, ref: female	-17.16 (-28.42, -5.9)	0.003	-13.56 (-24.44, -2.69)	0.015
Spherical refractive error, diopters	-3.8 (-6.71, -0.88)	0.01	-4.13 (-6.88, -1.39)	0.003
Intraocular pressure, mm Hg	-1.86 (-3.97, 0.25)	0.08	-1.72 (-3.74, -0.31)	0.1
Axial length, mm	0.61 (-4.35, 5.58)	0.81	2.08 (-2.5, 6.67)	0.37
Vertical cup-disc ratio	-267.14 (-310.52, -223.76)	<0.001	-256.79 (-298.05, -215.53)	<0.001
Retinal nerve fiber layer thickness, μ m	1.8 (1.25, 2.36)	<0.001	1.77 (1.26, 2.29)	<0.001
Rim area, mm ²	155.26 (131.57, 178.95)	<0.001	151.55 (129.66, 173.44)	<0.001
Disc area, mm ²	-46.46 (-63.28, -29.65)	<0.001	-46.27 (-62.17, -30.36)	<0.001
Mean deviation of SAP, dB	0.23 (-1.42, 1.88)	0.79	0.26 (-1.42, 1.94)	0.76
Pattern standard deviation of SAP (dB)	-4.23 (-6.98, -1.48)	0.003	-4.35 (-6.99, -1.72)	0.001

Bold typeface indicates the statistically significant values ($P < 0.05$).

* BMO-MRW₃₆ is Bruch's membrane opening-minimum rim width derived from 36 B-scans, whereas BMO-MRW₄ is from 4 B-scans.

TABLE 3. Multivariate Analysis of Bruch's Membrane Opening-Minimum Rim Width of Optic Nerve Head

Variables, <i>n</i> = 446	Multivariate Analysis of *BMO-MRW ₄		Multivariate Analysis of *BMO-MRW ₃₆	
	β (95% CI)	<i>P</i> Value	β (95% CI)	<i>P</i> Value
Age, y	-0.32 (-0.97, 0.34)	0.34	-0.2 (-0.8, 0.41)	0.53
Sex, ref: female	-5.4 (-11.18, 0.38)	0.07	-1.75 (-7, 3.5)	0.52
Spherical refractive error, diopters	-1.65 (-3.66, 0.37)	0.11	-2.23 (-4.07, -0.39)	0.02
Intraocular pressure, mm Hg	-0.23 (-1.36, 0.9)	0.69	-0.01 (-1.03, 1)	0.98
Vertical cup-disc ratio	-46.21 (-88.08, -4.35)	0.03	-37.51 (-78.49, 3.47)	0.07
Retinal nerve fiber layer thickness, μ m	0.44 (-0.12, 1)	0.12	0.5 (0.02, 0.98)	0.04
Rim area, mm ²	196.62 (166.21, 227.02)	<0.001	194.31 (167.1, 221.51)	<0.001
Disc area, mm ²	-92.16 (-115.88, -68.44)	<0.001	-91.78 (-114.73, -68.84)	<0.001

Bold typeface indicates statistically significant values ($P < 0.05$).

* BMO-MRW₃₆ is Bruch's membrane opening-minimum rim width derived from 36 B-scans, whereas BMO-MRW₄ is from 4 B-scans.

except for a marginal association with pulse pressure (defined as systolic - diastolic blood pressure) ($\beta = -0.46$, $P = 0.04$) (data not shown). This trend of associations of BMO-MRW was also observed even after reduction of B-scan analysis from 36 (72 BMO points, 5° interval) to 4 (8 BMO points, 90° interval) B-scans.

After adjusting for factors associated with BMO-MRW such as age, sex, IOP, and VCDR, BMO-MRW was found to be highly

associated with OCT-derived DA ($\beta = -91.78$, $P < 0.001$) and RA ($\beta = 194.31$, $P < 0.001$), followed by spherical refractive error ($\beta = -2.23$, $P = 0.02$) and RNFL thickness ($\beta = 0.5$, $P = 0.04$). Figure 2 shows a Bland-Altman plot comparing BMO-MRW measurements computed from 36 B-scans and from 4 B-scans. Limits of agreement (LOA) for BMO-MRW variability was -26.89 to 23.67, and the arithmetic mean was -1.61. Figure 3 shows the scatter plot of BMO-MRW against age of the subjects,

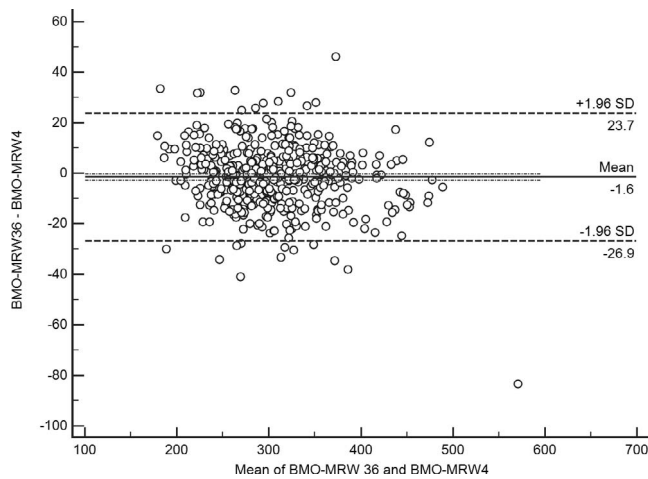


FIGURE 2. Bland-Altman plot comparing Bruch's membrane opening-minimum rim width computed from 36 B-scans and 4 B-scans.

demonstrating the linear relationship between decreasing BMO-MRW and increasing age ($P < 0.001$).

Bruch's membrane opening-MRW was significantly different among the sectors [temporal ($219.93 \pm 55.63 \mu\text{m}$) < superior-temporal ($318.04 \pm 66.3 \mu\text{m}$) < nasal ($319.53 \pm 72.69 \mu\text{m}$) < inferior-temporal ($324.5 \pm 69.24 \mu\text{m}$) < superior-nasal ($345.91 \pm 71.6 \mu\text{m}$) < inferior-nasal ($362.43 \pm 75.14 \mu\text{m}$) ($P < 0.001$)] except among superior-temporal, inferior-temporal, and nasal sectors (Fig. 4). Univariate analysis of sectoral BMO-MRW with clinical and imaging parameters revealed that sectoral BMO-MRW was highly associated with VCDR, RNFL, RA, and DA ($P < 0.001$) except the association of inferior-nasal sector BMO-MRW with RNFL thickness (Table 4).

DISCUSSION

Accurate measurement of the optic disc margin to determine the neuroretinal rim width, a surrogate for the ganglion cell

density within the eye, is fundamental for screening, diagnosis, and monitoring of glaucoma. In vivo imaging with SD-OCT provides a more objective assessment of ONH, particularly the disc margin, by using a consistent anatomical landmark, the BMO, compared to the subjective clinical identification of optic disc margin. A database of normal values of the BMO-MRW is needed with a large sample size for more accurate assessment of glaucoma diagnosis using this novel parameter. Chauhan et al.⁷ have suggested that BMO-MRW has higher diagnostic sensitivity and specificity than the current OCT-derived NRR measurement in POAG ($n = 107$) and normal controls ($n = 48$). The robustness of this parameter for diagnostic classification requires the availability of large and representative normative databases. This paper reports the results of a large dataset from a normal Chinese population.

We found that mean BMO-MRW was $304.67 \pm 58.96 \mu\text{m}$ with range 173.32 to 529.23 μm . It had, as expected, a positive association with RNFL thickness and RA, whereas it had a negative association with age, sex, spherical refractive error, VCDR, DA, and PSD. After adjusting for the above associated factors, BMO-MRW was positively associated with RA and RNFL thickness but negatively associated with DA and spherical refractive error.

Bruch's membrane opening-MRW was also significantly different among the six sectors (temporal, nasal, superior-temporal, superior-nasal, inferior-temporal, and inferior-nasal). Sectoral BMO-MRW was positively associated with RNFL thickness and RA while it was negatively associated with VCDR and DA. Pollet-Villard et al.¹⁶ reported that the structure-function relationship was stronger with BMO-MRW than RNFL or NRR by the built-in Cirrus algorithm when comparing the OCT-derived RNFL, NRR by built-in software, and NRR by BMO-MRW in six sectors with visual field sensitivity in the corresponding areas. They also found that NRR measured by either BMO-MRW or built-in Cirrus algorithm had better correlation with the retinal sensitivity in advanced glaucoma cases than the RNFL, while the RNFL measurement was better correlated with retinal sensitivity in the early stages of glaucoma. Most recently Danthurebandara et al.¹⁷ reported that relatively stronger global and sectoral structure-functional

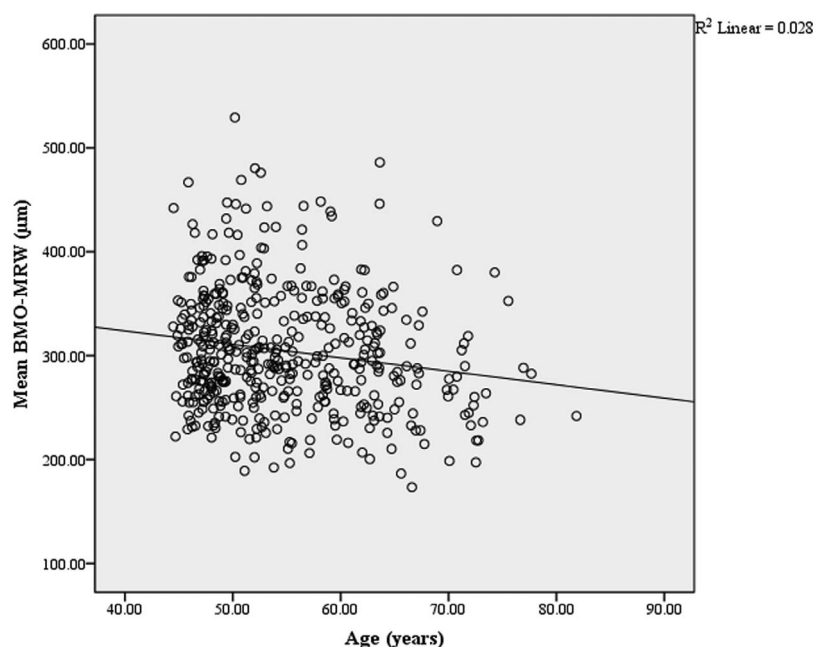


FIGURE 3. Scatterplot of mean Bruch's membrane opening-minimum rim width (μm) against age of participants (years).

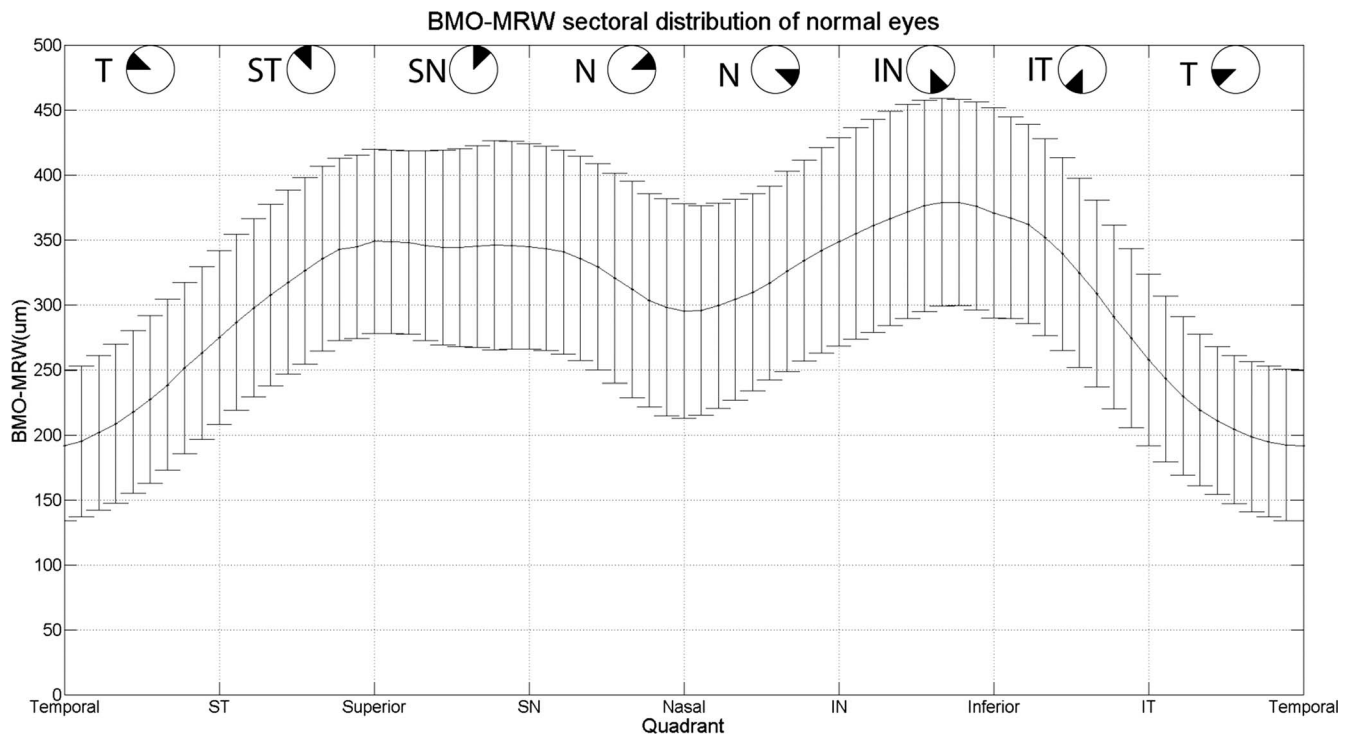


FIGURE 4. Sectoral distribution of Bruch's membrane opening-minimum rim width of all study participants.

relationships were obtained with BMO-MRW compared with clinical disc margin-based RA or BMO-horizontal rim width because of BMO-MRW's geometrically accurate properties.

In this cohort, BMO-MRW decreased with increasing age and was thicker in female subjects. The age-related loss of retinal ganglion cells (RCGs) has been estimated at 7209 RCGs per year, based on histological studies.¹⁸⁻²⁰ Bruch's membrane opening-MRW may be considered a surrogate of the number of RCGs within the disc, so it is encouraging to confirm an age-associated decline in this parameter. Patel et al.²¹ predicted that the loss of NRR based on BMO-MRW would be at 0.81 µm per year, assuming that all axons were sampled in cross section. This BMO-MRW decrease may also be due in part to angular bending of the BMO by tension on the axonal fibers by age-related differences in connective tissues such as the lamina cribrosa and sclera. The axial length of an eye may also have an

effect on ONH neuronal measurements because there may be stretching of BMO in longer eyes. There was no significant association of BMO-MRW with axial length in this study, although eyes with extremes of axial length were not included in this dataset.

There was no significant difference between the measurements computed from 36 B-scans and the cardinal 4 B-scans even after adjusting for age, sex, IOP, and other significant factors. Narrow LOA and small magnitude of mean bias from Bland-Altman analysis revealed that the BMO-MRW measurements from 36 B-scans and from 4 B-scans were comparable. These data suggest that the measurement of ONH could effectively be accomplished by using just the 4 cardinal B-scans for screening of a large population or for fast assessment in the clinic setting. However, this result should be cautiously interpreted because the use of fewer B-scans may fail to detect

TABLE 4. Univariate Analysis of Sectoral Bruch's Membrane Opening-Minimum Rim Widths With Demographic and Clinical Parameters

	Temporal		Inferior-Temporal		Inferior-Nasal		Superior-Temporal		Superior-Nasal		Nasal	
	β	P Value	β	P Value	β	P Value	β	P Value	β	P Value	β	P Value
Age, y	-0.59	0.08	-0.27	0.53	-0.49	0.4	-0.31	0.47	-0.2	0.66	-0.5	0.21
Sex, ref: female	-1.93	0.73	-11.81	0.06	-9.38	0.28	-7.94	0.23	-7.32	0.28	-2.5	0.69
Spherical refractive error, diopters	-2.07	0.1	-2.03	0.11	-6.05	<0.01	-1.97	0.18	-1.04	0.48	-1.94	0.16
Intraocular pressure, mm Hg	-0.29	0.78	-1.08	0.41	-1.95	0.28	-1.92	0.11	-1.2	0.36	-0.88	0.47
Vertical cup-disc ratio	-103.7	<0.01	-123.32	<0.01	-128.83	<0.01	-112.2	<0.01	-131.05	<0.01	-101.71	<0.01
Retinal nerve fiber layer thickness, µm	0.55	<0.05	1.12	<0.01	0.68	0.12	0.95	<0.01	1.04	<0.01	1.14	<0.01
Rim area, mm ²	44.9	<0.01	65.92	<0.01	57.14	<0.01	71.33	<0.01	88.83	<0.01	72.81	<0.01
Disc area, mm ²	-31.67	<0.01	-26.05	<0.01	-32.33	<0.01	-41.35	<0.01	-30.85	<0.01	-29.98	<0.01

Bold typeface indicates statistically significant values ($P < 0.05$).

localized changes of ONH. Regional variability of ONH is more likely to be detected by a higher density of B-scans. By the same token, this strategy may fail to detect progression of disease due to lack of information in between scans.

Limitations of this study include the fact that the built-in Cirrus OCT algorithm may in itself have segmentation error when detecting BMO (around 10% subjective assessment by the authors). The customized algorithm we developed has not been validated yet in another subject group and may also therefore be subject to calculation error. Furthermore, our algorithm does not link the center of the BMO to the angular location of the fovea, as is now performed using the Heidelberg Engineering Glaucoma Premium Edition.²² This likely means that there will be some errors in the sectoral measurements as certain sectors will be incorrectly aligned, depending on the location of the fovea. However, this effect is likely to be small and to have no influence on the global or mean measurements. The current study population was Chinese, and therefore the results may not be comparable to those for other ethnic groups. A more comprehensive normative database of BMO-MRW should include measurements for subjects aged 18 to 40 years, data that were not available in this study. Furthermore, subjects with cataract were not excluded, and it is possible that the presence of cataract may affect the results of OCT imaging.²³ However, all the images had high signal strength, indicating that the presence of cataract likely had minimal impact.

The present study demonstrates that BMO-MRW has positive association with OCT-derived RA and RNFL while it has negative association with OCT-derived DA and spherical refractive error. This normative database of BMO-MRW will facilitate more accurate optic nerve head assessment in Chinese subjects using Cirrus OCT.

Acknowledgments

The authors thank Benjamin Adam Haaland for advising on statistical methods.

Supported by Biomedical Research Council Grant 08/1/35/19/550, Singapore; the Ministry of Education, Academic Research Funds, Tier 1 (R-397-000-140-133) and an NUS Young Investigator Award (NUSYIA-FY13-P03; R-397-000-174-133) (MJAG). Supported in part by the United Kingdom Department of Health through the award made by the National Institute for Health Research to Moorfields Eye Hospital NHS Foundation Trust and UCL Institute of Ophthalmology for a Biomedical Research Centre for Ophthalmology (NGS). The views expressed in this publication are those of the authors and not necessarily those of the UK Department of Health. The sponsor or funding organization had no role in the design or conduct of this research.

Disclosure: **T.A. Tun**, None; **C.-H. Sun**, None; **M. Baskaran**, None; **M.J.A. Girard**, None; **J.M.S. de Leon**, None; **C.-Y. Cheng**, None; **H.M. Htoon**, None; **T.Y. Wong**, None; **T. Aung**, None; **N.G. Strouthidis**, None

References

- Strouthidis NG, Yang H, Fortune B, et al. Detection of optic nerve head neural canal opening within histomorphometric and spectral domain optical coherence tomography data sets. *Invest Ophthalmol Vis Sci*. 2009;50:214-223.
- Strouthidis NG, Yang H, Reynaud JF, et al. Comparison of clinical and spectral domain optical coherence tomography optic disc margin anatomy. *Invest Ophthalmol Vis Sci*. 2009;50:4709-4718.
- Reis AS, Sharpe GP, Yang H, et al. Optic disc margin anatomy in patients with glaucoma and normal controls with spectral domain optical coherence tomography. *Ophthalmology*. 2012;119:738-747.
- Povazay B, Hofer B, Hermann B, et al. Minimum distance mapping using three-dimensional optical coherence tomography for glaucoma diagnosis. *J Biomed Opt*. 2007;12:041204.
- Chen TC. Spectral domain optical coherence tomography in glaucoma: qualitative and quantitative analysis of the optic nerve head and retinal nerve fiber layer (an AOS thesis). *Trans Am Ophthalmol Soc*. 2009;107:254-281.
- Strouthidis NG, Fortune B, Yang H, et al. Longitudinal change detected by spectral domain optical coherence tomography in the optic nerve head and peripapillary retina in experimental glaucoma. *Invest Ophthalmol Vis Sci*. 2011;52:1206-1219.
- Reis AS, O'Leary N, Yang H, et al. Influence of clinically invisible, but optical coherence tomography detected, optic disc margin anatomy on neuroretinal rim evaluation. *Invest Ophthalmol Vis Sci*. 2012;53:1852-1860.
- Chauhan BC, O'Leary N, Almobarak FA, et al. Enhanced detection of open-angle glaucoma with an anatomically accurate optical coherence tomography-derived neuroretinal rim parameter. *Ophthalmology*. 2013;120:535-543.
- Abràmoff MD, Lee K, Niemeijer M, et al. Automated segmentation of the cup and rim from spectral domain OCT of the optic nerve head. *Invest Ophthalmol Vis Sci*. 2009;50:5778-5784.
- Mwanza JC, Oakley JD, Budenz DL, Anderson DR; Cirrus Optical Coherence Tomography Normative Database Study Group. Ability of cirrus HD-OCT optic nerve head parameters to discriminate normal from glaucomatous eyes. *Ophthalmology*. 2011;118:241-248.
- Gardiner SK, Ren R, Yang H, et al. A method to estimate the amount of neuroretinal rim tissue in glaucoma: comparison with current methods for measuring rim area. *Am J Ophthalmol*. 2014;157:540-549, e1-e2.
- Lavanya R, Jeganathan VS, Zheng Y, et al. Methodology of the Singapore Indian Chinese Cohort (SICC) eye study: quantifying ethnic variations in the epidemiology of eye diseases in Asians. *Ophthalmic Epidemiol*. 2009;16:325-336.
- Gupta P, Sidhartha E, Tham YC, et al. Determinants of macular thickness using spectral domain optical coherence tomography in healthy eyes: the Singapore Chinese Eye study. *Invest Ophthalmol Vis Sci*. 2013;54:7968-7976.
- Tham YC, Cheung CY, Koh VT, et al. Relationship between ganglion cell-inner plexiform layer and optic disc/retinal nerve fibre layer parameters in non-glaucomatous eyes. *Br J Ophthalmol*. 2013;97:1592-1597.
- Moghimi S, Hosseini H, Riddle J, et al. Measurement of optic disc size and rim area with spectral-domain OCT and scanning laser ophthalmoscopy. *Invest Ophthalmol Vis Sci*. 2012;53:4519-4530.
- Pollet-Villard F, Chiquet C, Romanet JP, et al. Structure-function relationships with spectral-domain optical coherence tomography retinal nerve fiber layer and optic nerve head measurements. *Invest Ophthalmol Vis Sci*. 2014;55:2953-2962.
- Danthurebandara VM, Sharpe GP, Hutchison DM, et al. Enhanced structure-function relationship in glaucoma with an anatomically and geometrically accurate neuroretinal rim measurement. *Invest Ophthalmol Vis Sci*. 2014;56:98-105.
- Balazsi AG, Rootman J, Drance SM, et al. The effect of age on the nerve fiber population of the human optic nerve. *Am J Ophthalmol*. 1984;97:760-766.
- Repka MX, Quigley HA. The effect of age on normal human optic nerve fiber number and diameter. *Ophthalmology*. 1989;96:26-32.
- Mikelberg FS, Drance SM, Schulzer M, et al. The normal human optic nerve. Axon count and axon diameter distribution. *Ophthalmology*. 1989;96:1325-1328.

21. Patel NB, Lim M, Gajjar A, et al. Age-associated changes in the retinal nerve fiber layer and optic nerve head. *Invest Ophthalmol Vis Sci.* 2014;55:5134-5143.
22. Heidelberg Engineering. Glaucoma Premium Edition. Anatomic Positioning System (APS). Heidelberg Engineering, Germany. Available at: <http://www.heidelbergengineering.com/international/products/spectralis/key-features/glaucoma-module-premium-edition/>. Accessed December 22, 2014.
23. Kok PH, van den Berg TJ, van Dijk HW, et al. The relationship between the optical density of cataract and its influence on retinal nerve fibre layer thickness measured with spectral domain optical coherence tomography. *Acta Ophthalmol.* 2013;91:418-424.